Check for updates

A Journal of the Gesellschaft Deutscher Chemiker

Angewandte International Edition GDCh Chemie

www.angewandte.org

Accepted Article

Title: Regulation of Redox Molecular Junctions in Covalent Organic Frameworks for H2O2 Photosynthesis Coupled with Biomass Valorization

Authors: Jia-Nan Chang, Jing-Wen Shi, Qi Li, Shan Li, Yi-Rong Wang, Yifa Chen, Fei Yu, Shun-Li Li, and Ya-Qian Lan

This manuscript has been accepted after peer review and appears as an Accepted Article online prior to editing, proofing, and formal publication of the final Version of Record (VoR). The VoR will be published online in Early View as soon as possible and may be different to this Accepted Article as a result of editing. Readers should obtain the VoR from the journal website shown below when it is published to ensure accuracy of information. The authors are responsible for the content of this Accepted Article.

To be cited as: *Angew. Chem. Int. Ed.* **2023**, e202303606

Link to VoR: https://doi.org/10.1002/anie.202303606

WILEY VCH

10.1002/anie.202303606

WILEY-VCH

RESEARCH ARTICLE

Regulation of Redox Molecular Junctions in Covalent Organic Frameworks for H_2O_2 Photosynthesis Coupled with Biomass Valorization

Jia-Nan Chang[a], Jing-Wen Shi[a], Qi Li[a], Shan Li[a], Yi-Rong Wang[b], Yifa Chen[b]*, Fei Yu[a]*, Shun-Li Li[b], Ya-Qian Lan[b]*

[a] Dr. J.-N. C., J.-W. S., Q. L., S. L. and Prof. F. Y.
Jiangsu Collaborative Innovation Centre of Biomedical Functional Materials, Jiangsu Key Laboratory of New Power Batteries, School of Chemistry and Materials Science
Nanjing Normal University
Nanjing 210023, P. R. China
[b] Dr. Y.-R. W., Prof. Y. C., Prof. S.-L. L. and Prof. Y.-Q. L.
School of Chemistry, South China Normal University, Guangzhou, 510006, P. R. China
E-mail: chyf927821@163.com; E-mail: feiyu@njnu.edu.cn; E-mail: yqlan@njnu.edu.cn; yqlan@m.scnu.edu.cn

Supporting information for this article is given via a link at the end of the document.

Abstract: The H_2O_2 photosynthesis coupled with biomass-valorization can not only maximize the energy utilization but also realize the production of value-added products. Here, a series of COFs (i.e. Cu_3-BT-COF, Cu_3-pT-COF and TFP-BT-COF) with regulated redox molecular junctions have been prepared to study the H_2O_2 photosynthesis coupled with furfuryl alcohol (FFA) photo-oxidation to furoic acid (FA). Best of them, the FA generation-efficiency of Cu_3-BT-COF can be 575 mM g^{-1} (conv. ~100% and sele. >99%) and meanwhile the H_2O_2 production-rate can reach up to 187,000 μM g^{-1}, much higher than Cu_3-pT-COF, TFP-BT-COF and its monomers. As proved by theoretical calculations, the covalent coupling of Cu cluster and thiazole group can promote the charge-transfer, substrate-activation and FFA-dehydrogenation, thus boosting the both kinetics of H_2O_2 production and FFA photo-oxidation to increase the efficiency. This is the first work about COFs for H_2O_2 photosynthesis coupled with biomass-valorization, which might facilitate the exploration of porous-crystalline-catalysts in this field.

Introduction

Hydrogen peroxide (H_2O_2), as a benign oxidant, has attracted intensive attention in wastewater treatment, disinfection and paper industry, etc.[1] From the supply and demand of H_2O_2, the China's annual production of high-purity H_2O_2 has reached >100,000 tons and meanwhile the global demand of H_2O_2 has reached up to about US$5.5 billion by 2023.[2] Anthraquinone (AQ) oxidation method is the main method for industrial production of H_2O_2 at present, yet the AQ reaction process is complex with the utilization of a large amount of organic solvents, which is contrary to the concept of sustainable development.[3] In this regard, it is desired to develop more efficient and greener H_2O_2 production methods to meet the unmet growing demand. As an environmentally benign catalytic system, H_2O_2 photosynthesis has attracted a lot of attention around the world.[4a] Specifically, the ideal H_2O_2 photosynthesis system only needs abundant water and oxygen on the earth as raw materials, and uses sunlight as green energy to activate photocatalysts.[4] During the detailed mechanistic process, oxygen reduction reaction (ORR) and water oxidation reaction (WOR) are two vital half reactions that can simultaneously produce H_2O_2 driven by photocatalysts.[5] However, the light-driven $2e^-$ WOR pathway is not easy to achieve due to the uphill thermodynamics (1.76 V versus normalized hydrogen electrode, NHE) when compared with that of ORR.[6] In general, the balance between WOR and ORR is very important for the production of H_2O_2 as they can synergistically determine the catalytic kinetics and efficiency.[7a] In order to adjust the challenge issues of WOR, the sacrificial agent oxidation method has been developed to replace WOR and most of sacrificial agents are based on alcohols (e.g., methanol, ethanol, isopropanol and benzyl alcohol, etc.).[7b] However, the sacrificial agent oxidation method still faces some shortcomings: i) the sacrificial agent oxidation method would reduce both of the H_2O_2 generation and total energy utilization efficiency due to the single generation pathway through ORR; ii) most of sacrificial agents like alcohols in higher values will be transferred into aldehyde or acid with lower ones and lack in the economic benefits and iii) the utilization of sacrificial agents will result in complex products during the process and increase the difficulty in product purification or mechanism study.[8] Thus, more attractive oxidation reactions would still be needed to be coupled with ORR to precisely design powerful H_2O_2 photosynthesis coupled systems for both value-added products (e.g., oxidation products and H_2O_2) and maximized total energy utilization efficiency.

Biomass valorization plays a positive role in solving energy and environmental crisis, which can generate high value-added products in a green and pollution-free way for future sustainable development.[9] Especially for the photocatalytic conversion of biomass, a mild and green approach, can achieve the photocatalytic valorization of biomass into high value-added products to meet the potentially sustainable target.[9b,c] Thus, the combination of photocatalytic biomass valorization with H_2O_2 photosynthesis would be a desired strategy to fulfill above-mentioned requirements. Furfuryl alcohol (FFA), as a traditional biomass, has be utilized for the syntheses of a series of pharmaceuticals, monomers and fine chemicals (e.g., furfural (FF) or furoic acid (FA), etc.). Among them, FA as a kind of important product can serve as raw material for the syntheses of multiple intermediates (e.g., methyl furan, fur furamide, furoate, plasticizer and thermosetting resin, etc.) in plastic industry or preservatives in food industry.[10] According to the above analysis, if the photocatalytic valorization of FFA can be combined with H_2O_2 photosynthesis, it would maximize the total energy utilization to

This article is protected by copyright. All rights reserved.

15213773, ja, Downloaded from https://onlinelibrary.wiley.com/doi/10.1002/anie.202303606 by South China Normal University, Wiley Online Library on [13/06/2023]. See the Terms and Conditions (https://onlinelibrary.wiley.com/terms-and-conditions) on Wiley Online Library for rules of use; OA articles are governed by the applicable Creative Commons License

Accepted Manuscript

10.1002/anie.202303606

produce value-added products of both FA and H_2O_2. Up to date, there are some pioneering works about the H_2O_2 photosynthesis coupled with FFA photo-oxidation and related photocatalysts like TiO_2 or its hybrid derivatives have been reported.[11] However, their applications in the photocatalytic coupled system still face drawbacks: i) TiO_2 has wide bandgap (3.2 eV) and requires UV light (< 5% of solar illumination) for photo-activation[11c,12]; ii) due to the lack in precise regulation of photo-redox ability, the furan ring of FFA might be over or insufficiently oxidated, thus leading to the formation of undesired products with low efficiency[13]; iii) most of them are in nonporous solid-particle forms, resulting in less-exposed catalytic sites and are not conducive to substrate adsorption or mass transfer[14] and iv) most of them are in non-crystalline or hybridized forms that would increase the difficulty in detailed mechanism study.[15] In addition to these issues, the design of suitable photocatalysts for H_2O_2 photosynthesis coupled with FFA photo-oxidation still needs stringent requirements (e.g., suitable band gaps, photo-redox property, light absorbance ability and effective electron-hole separation efficiency, etc.), which would set high bottlenecks for this filed. Therefore, it would be much essential to design powerful photocatalysts that can conquer the drawbacks and meet the stringent requirements to realize the photocatalytic coupled system to simultaneously produce H_2O_2 and value-added biomass derivatives.

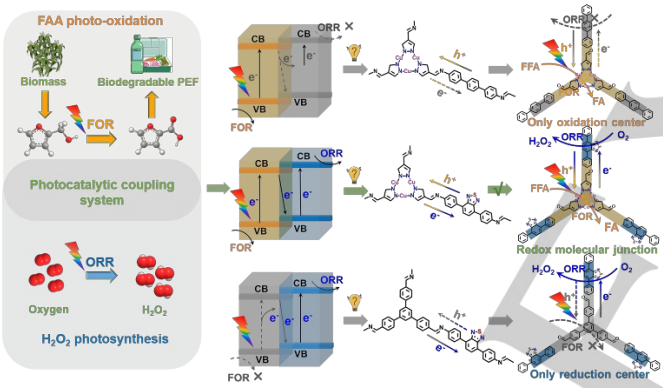

Scheme 1. Schematic representation of redox molecular junction COFs for H_2O_2 photosynthesis coupled with FFA photo-oxidation.

Covalent organic frameworks (COFs), composed of light-weight elements and linked by covalent bonds, present crystalline structures, tunable functionality, high stability and porosity, etc.[16] Recently, metal cluster-based COFs (MCOFs), a kind of attractive COFs obtained through the covalent connection between metal clusters and organic molecules[17], have showed high promise in many applications like CO_2 photo-reduction[18], photocatalytic cycloaddition of CO_2[19], or photo-oxidation of biomass[17c], etc. Specifically, the pre-designable metal clusters can be covalently connected with organic linkers to endow MCOFs with intrinsic properties and might be applied as potential photocatalysts for the H_2O_2 photosynthesis coupled with FFA photo-oxidation owing to the following reasons: i) compared with other materials with higher density, MCOFs with low density and high porosity might provide more exposed surface area and active sites that can be assessable for the substrates[17d]; ii) the tunable structures with functional struts endow MCOFs with efficient metal-ligand charge transfer (MLCT) effect to realize efficient separation of electrons and holes to accomplish the coupled reaction[20] and iii) MCOFs with crystalline and well-defined structures are conducive to mechanism study. However, the applications of MCOFs in H_2O_2 photosynthesis coupled with FFA photo-oxidation are still rare as far as we known. In this regard, the design of novel and powerful MCOFs with multi-functionality that can meet the requirements for the photocatalytic coupled system is highly demanded to realize the simultaneous FFA-to-FA and H_2O_2 generation.

Herein, we have prepared a series of redox molecular junction COFs (i.e. Cu_3-BT-COF, Cu_3-pT-COF and TFP-BT-COF) with different functional groups to study the H_2O_2 photosynthesis coupled with FFA photo-oxidation (Scheme 1). Among them, Cu_3-BT-COF as a kind of newly designed MCOF with nanosheet morphology (~1.25 nm) constructed by the covalent connection of Cu_3 and thiazole group (BT) exhibits the optimal photocatalytic coupled reaction properties. Specifically, the covalent connection between Cu_3 and BT in Cu_3-BT-COF enables the visible light driven electron-hole to efficiently separate and transfer from Cu_3 to BT moiety, resulting in the photoexcited electrons (on BT) and holes (on Cu_3) that can be applied for H_2O_2 photosynthesis and FFA photo-oxidation reactions, respectively. Notably, the FA generation efficiency of Cu_3-BT-COF can be as high as 575 mM g^{-1} (conv. ~100% and sele. >99%) and meanwhile the H_2O_2 production rate can reach up to 187,000 μM g^{-1}, much higher than Cu_3-pT-COF, TFP-BT-COF and its monomers. In addition, the reaction presents high versatility and can be extended to other alcohol photo-oxidation systems like H_2O_2 photosynthesis coupled with 2-thiophenemethanol photo-oxidation.

For the synthesis of Cu_3-BT-COF, $Cu_3(PyCA)_3{\cdot}H_2O$ (denoted as Cu_3, PyCA stands for pyrazole-4-carbaldehyde) has been initially synthesized by using $Cu(NO_3)_2{\cdot}3H_2O$ and 1H pyrazole-4-acetaldehyde (HPyCA) as raw materials through solvothermal method (detail see Methods).[21] Afterwards, Cu_3-BT-COF is synthesized by Schiff-base condensation between Cu_3 and 4,4′-(benzo-2,1,3-thiadiazole-4,7-diyl)dianiline (BT-NH_2) through a solvothermal method and a kind of reddish brown powder is obtained after 72 h at 120 °C (Figure 1a and Figure S1). The crystalline structure of Cu_3-BT-COF is defined by the powder X-ray diffraction (PXRD) combined with theoretical structural simulations. The R_3 space group based on Cu_3-BT-COF is constructed and performed Le Bail refinements of the PXRD patterns for full profile fitting against the proposed models, which gives a unit cell parameter of a = 47.65 Å, b = 47.65 Å, and c = 2.60 Å, α = β = 90°, γ = 120° (Table S1). Moreover, the simulated PXRD pattern applying ABC stacking mode reproduce the experimentally observed curve while AB stacking does not, which is verified by the difference plot with unweighted-profile R factor (Rp) of 2.42% and weighted profile R factor (Rwp) of 3.16%, respectively (Figure 1c and e). In addition, Fourier transform infrared spectroscopy (FTIR) is utilized to characterize the chemical structure of Cu_3-BT-COF. In the FTIR spectra, the C=N stretching vibration at 1620 cm^{-1} appears in the resultant Cu_3-BT-COF (Figure S2) [2b], suggesting the successful formation of Cu_3-BT-COF.

To investigate the chemical states of the existed elements in Cu_3-BT-COF, X-ray photoelectron spectroscopy (XPS) measurements have been carried out. For the XPS spectra of Cu_3-BT-COF, five main peaks with binding energy of 933.69, 164.55, 284.54, 399.12 and 531.46 eV are ascribed to Cu 2p, S 2p, C 1s, N 1s and O 1s, respectively (Figure S3). In the Cu 2p region, two kinds of peaks with binding energy of 935.03 and

This article is protected by copyright. All rights reserved.

15213773, ja, Downloaded from https://onlinelibrary.wiley.com/doi/10.1002/anie.202303606 by South China Normal University, Wiley Online Library on [13/06/2023]. See the Terms and Conditions (https://onlinelibrary.wiley.com/terms-and-conditions) on Wiley Online Library for rules of use; OA articles are governed by the applicable Creative Commons License

Accepted Manuscript

10.1002/anie.202303606

933.62 eV are assigned to Cu^{2+} and Cu^{+}, respectively, which is identical to previously reported studies.[21] Moreover, the XPS spectra of S, N and O elements of Cu_3-BT-COF are shown in Figure S4. The structural porosity and specific surface area of Cu_3-BT-COF are determined using nitrogen sorption tests at 77 K. N_2 adsorption-desorption curves exhibit a typical reversible isotherm, revealing the presence of micropores for Cu_3-BT-COF (Figure S5). Besides, the Brunauer-Emmett-Teller surface area (S_{BET}) of Cu_3-BT-COF is calculated to be 186 m^2 g^{-1}. Similarly, Cu_3-pT-COF and TFP-BT-COF have also prepared as the contrast samples of Cu_3-BT-COF and characterized (Figure 1b, d, Figures S6-9 and Table S2-3).

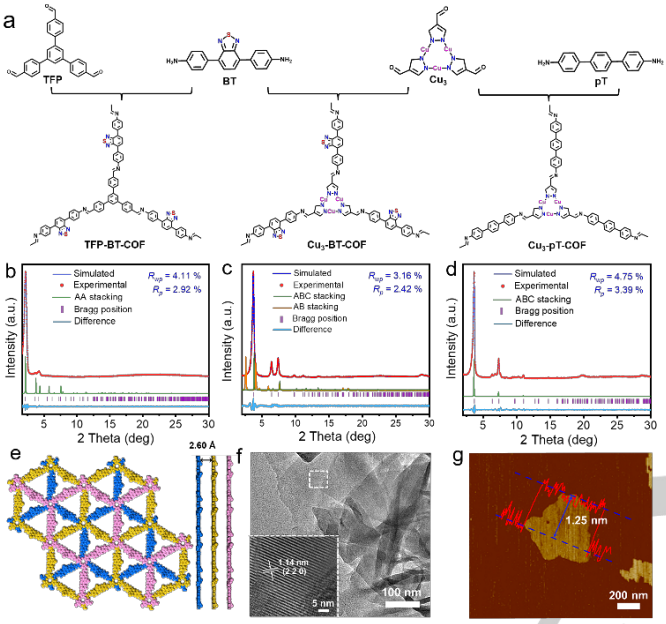

Figure 1. Structure and characterization of Cu_3-BT-COF. (a) Schematic representation of the syntheses of Cu_3-BT-COF, Cu_3-pT-COF and TFP-BT-COF. (b - d) Experimental (red dot) and simulated (blue line) PXRD patterns of Cu_3-BT-COF (c), Cu_3-pT-COF (d) and TFP-BT-COF (b). (e) Top and side views of the structure of Cu_3-BT-COF. (f) The HRTEM image and lattice fringes of Cu_3-BT-COF (inset is taken from the section highlighted in f). (g) Atomic force microscope (AFM) image and height profile of Cu_3-BT-COF.

Besides, we have carried out the atomic force microscope (AFM) tests to evaluate the thickness and morphology of Cu_3-BT-COF. In the AFM image, Cu_3-BT-COF shows nanosheet morphology (size, ~600 nm) and the thickness is calculated to be ~1.25 nm in the height profile (Figure 1g). In addition, the nanosheet morphology is further confirmed by the TEM test (Figure 1f). Specifically, the oriented lattice fringes can be observed in the high-resolution TEM (HR-TEM) image and the lattice spacing of 1.14 nm is assigned to the (2 2 0) plane (inset image, Figure 1f). Additionally, elemental mapping analysis reveals that Cu, N and S are uniformly distributed in Cu_3-BT-COF (Figure S10). Furthermore, we have also characterized the morphology of Cu_3-pT-COF and TFP-BT-COF by SEM and TEM tests (Figure S11-12).

To investigate the chemical stability of Cu_3-BT-COF, the samples are soaked in diverse kinds of solvents (i.e., N, N-dimethylformamide, acetonitrile, methanol and H_2O) for 5 days. After tests, the samples have been characterized by the PXRD and FTIR tests (Figure S13-14). The PXRD results before and after the experiments show that the crystallinity of Cu_3-BT-COF immersed in different solutions remains intact. These results are also certified by the FTIR tests, indicating the high stability of these COFs and would set fundamental basis for photocatalytic applications.

Based on the ultraviolet and visible (UV-Vis) absorption spectra, Cu_3-BT-COF, Cu_3-pT-COF and TFP-BT-COF all have absorption in the visible light range (400 - 800 nm) (Figure 2a). The band gaps (E_g) of Cu_3-BT-COF, Cu_3-pT-COF and TFP-BT-COF are determined to be 1.92, 2.67 and 2.06 eV by their Tauc plots (Figure 2b). The highest occupied molecular orbital (HOMO) of Cu_3-BT-COF, Cu_3-pT-COF and TFP-BT-COF are determined by ultraviolet photoelectron spectroscopy (UPS), from which the HOMO of Cu_3-BT-COF is estimated to be -6.80 eV (*vs.* vacuum level, E_v) by subtracting the excitation energy of 21.22 eV from the width of the He I UPS spectrum.[22] Likewise, the HOMOs of Cu_3-pT-COF and TFP-BT-COF are determined to be -7.59 eV and -6.68 eV (*vs.* E_v), respectively (Figure S15-17). In order to verify the accuracy of these results, we have also carried out the Mott Schottky electrochemical measurements to analyze the energy band positions of Cu_3-BT-COF, Cu_3-pT-COF and TFP-BT-COF (Figure S18-20). Based on the results, the LUMO of Cu_3-BT-COF, Cu_3-pT-COF and TFP-BT-COF are calculated to be 0.04 V, 0.08 V, and -0.22 V (*vs.* NHE, pH 7), respectively. Meanwhile, the HOMO positions of Cu_3-BT-COF, Cu_3-pT-COF and TFP-BT-COF are 1.96 V, 2.75 V and 1.84 V (*vs.* NHE, pH 7), respectively, which are well associated with the UV-Vis absorption spectra (Figure 2e). Notably, these results are also consistent with the values obtained by UPS tests (Figure S15-20).

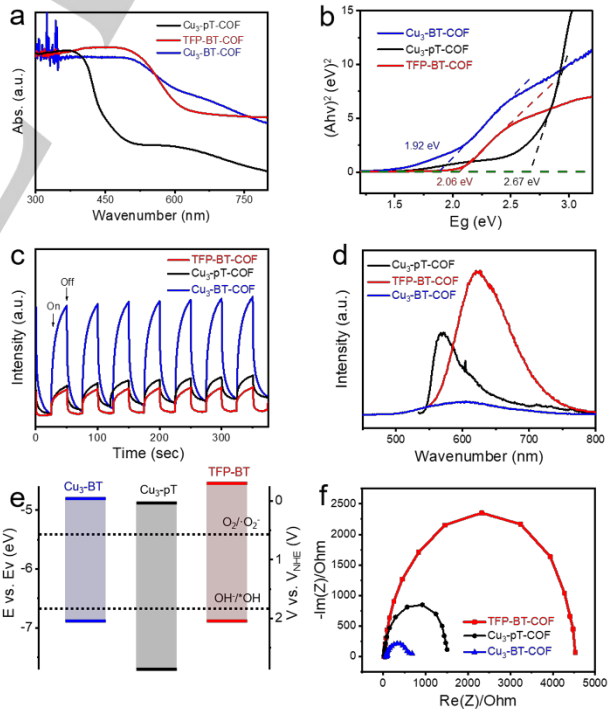

Figure 2. Characterizations of the optical properties for Cu_3-BT-COF, Cu_3-pT-COF and TFP-BT-COF. (a) UV-Vis absorption spectra. (b) Tauc plot for band gaps calculation. (c) Transient photocurrent response. (d) The steady-state photoluminescence (PL) measurements. (e) Band-structure diagram. (f) Nyquist plots.

This article is protected by copyright. All rights reserved.

15213773, ja, Downloaded from https://onlinelibrary.wiley.com/doi/10.1002/anie.202303606 by South China Normal University, Wiley Online Library on [13/06/2023]. See the Terms and Conditions (https://onlinelibrary.wiley.com/terms-and-conditions) on Wiley Online Library for rules of use; OA articles are governed by the applicable Creative Commons License

Accepted Manuscript

10.1002/anie.202303606

RESEARCH ARTICLE

During the process of the coupled reaction, there are two vital intermediates (i.e., *OH and O_2^-) that can significantly affect the H_2O_2 photosynthesis coupled with FFA photo-oxidation, thus it is very important to match the band structures of photocatalysts with the theoretical oxidation and reduction potentials for the photocatalytic coupled system.[11c] Obviously, the band structures of Cu_3-BT-COF, Cu_3-pT-COF and TFP-BT-COF are basically sufficient for the syntheses of *OH (E_{*OH/OH^-} = +1.76 V *vs* NHE) and O_2^- ($E_{O2-/O2}$ = +0.68 V *vs* NHE) as shown in Figure 2e.[23]

In addition, transient photocurrent response and steady-state photoluminescence (PL) measurements have been performed to investigate the charge-transfer behaviors (Figure 2d).[20] The transient photocurrent response intensity of Cu_3-BT-COF is much higher than those of Cu_3-pT-COF and TFP-BT-COF, as shown in Figure 2c. The steady-state photoluminescence (PL) of Cu_3-BT-COF is much lower than that of Cu_3-pT-COF and TFP-BT-COF (Figure 2d). In addition, time-resolved fluorescence decay spectra have been performed to evaluate the charge carrier dynamics. The longest average lifetime of Cu_3-BT-COF implies that the photogenerated charges in Cu_3-BT-COF can survive the longest to participate in the catalytic reaction (Figure S21). Additionally, the electrochemical impedance spectroscopy (EIS) has also conducted to investigate the charge transfer resistance (Figure 2f). The Nyquist plots demonstrate that Cu_3-BT-COF (533 Ω) has much smallest charge transfer resistance when compared with Cu_3-pT-COF (1519 Ω) and TFP-BT-COF (4440 Ω).[24] Moreover, the UV-Vis absorption and Mott Schottky electrochemical measurements have been also carried out on Cu_3 and BT monomers to determine their energy band positions for further performance comparison (Figure S22-24).

The experiments of H_2O_2 photosynthesis coupled with FAA photo-oxidation were carried out under pure O_2 atmosphere in aqueous solution with a certain amount of FAA added (Figure S25). The production rate of FA and H_2O_2 have been determined by high-performance liquid chromatography (HPLC) and iodometry methods, respectively (Figure S26-32).[25] In the presence of Cu_3-BT-COF, with the increase of reaction time (1 to 4 h), the conversion efficiency of FAA and the production rate of FA increase gradually (Figure 3b). After 4 h, the production rate of FA can reach up to 575 mM g^{-1} (conv. ~100% and sele. >99%), and meanwhile the production rate of H_2O_2 is as high as 187,000 μM g^{-1} (Figure 3a). The achieved performances for both of the products by Cu_3-BT-COF are comparable to most of TiO_2 based photocatalysts that only can generate one kind of product (Table S4 and S5).[11c,26]. In contrast, the FA production rate of Cu_3-pT-COF and TFP-BT-COF are 187 mM g^{-1} and 168 mM g^{-1}, respectively (Figure 3b). Notably, the H_2O_2 production rate of Cu_3-BT-COF can be 187,000 μM g^{-1}, much higher than Cu_3-pT-COF (64,600 μM g^{-1}) and TFP-BT-COF (94,000 μM g^{-1}) (Figure 3a). In contrast, the conversion efficiency for FAA of Cu_3, BT and physical mixture are tested to be 75%, 81% and 87%, respectively (Figure S33). At the same time, their production rates of H_2O_2 (i.e., Cu_3, 76,000 μM/h/g; BT, 34,000 μM/h/g and physical mixture, 62,000 μM/h/g) are also much lower than that of Cu_3-BT-COF (Figure S34).

In order to prove the superiority of this photocatalytic coupled system to traditional full reaction photosynthesis of H_2O_2, the comparative tests have been conducted (Figure S35). Under the O_2 atmosphere and pure water, the concentration of H_2O_2 gradually increases with the extension of illumination time (1 to 4 h), and finally reaches to 87,400 μM g^{-1}. Specifically, the production rate of H_2O_2 in the photocatalytic coupled reaction is more than 2 times higher than that of full reaction photosynthesis of H_2O_2. In addition, $^{18}O_2$ isotope experiments have been carried out to verify the ORR process for H_2O_2 photosynthesis (Figure 3f). Cu_3-BT-COF is illuminated in $H_2{}^{16}O$ and $^{18}O_2$ gas for 4 h. After removing the unreacted gas with Ar gas, MnO_2 is added to the reaction system to decompose H_2O_2 and release O_2. The escaped gas is analyzed by gas chromatography-mass spectrometry. The decomposition products are $^{18}O_2$ and $^{16}O_2$, in which $^{18}O_2$ accounts for the majority and shows that H_2O_2 is produced mainly through the ORR process by Cu_3-BT-COF (Figure 3f). Interestingly, a small amount of H_2O_2 can still be produced by the WOR process, as certified by the detection of trace $^{16}O_2$ from the decomposed H_2O_2 in the isotope experiment, which indicates it to be a competitive reaction between FFA photo-oxidation and WOR, and the dominate role of FFA photo-oxidation for the half reaction. Besides, the apparent quantum yield (AQY) between 420 nm is 7.98% with a solar chemical conversion (SCC) efficiency of 0.62%, which are much higher than the full reaction photosynthesis of H_2O_2 (AQY, 3.72% and SCC, 0.28%).

Besides, the cycling stability is a vital factor to evaluate the durability of the photocatalyst. After three cycles of photocatalytic tests, the catalytic performance remains almost unchanged, proving the high cycling stability of Cu_3-BT-COF (Figure S36-37). Furthermore, the structural integrity of Cu_3-BT-COF is also confirmed by both the PXRD and FTIR tests (Figure S38-39). In addition, Cu_3-pT-COF and TFP-BT-COF also exhibit high structural stability during the photocatalytic reaction as proved by the PXRD tests (Figure S40-41).

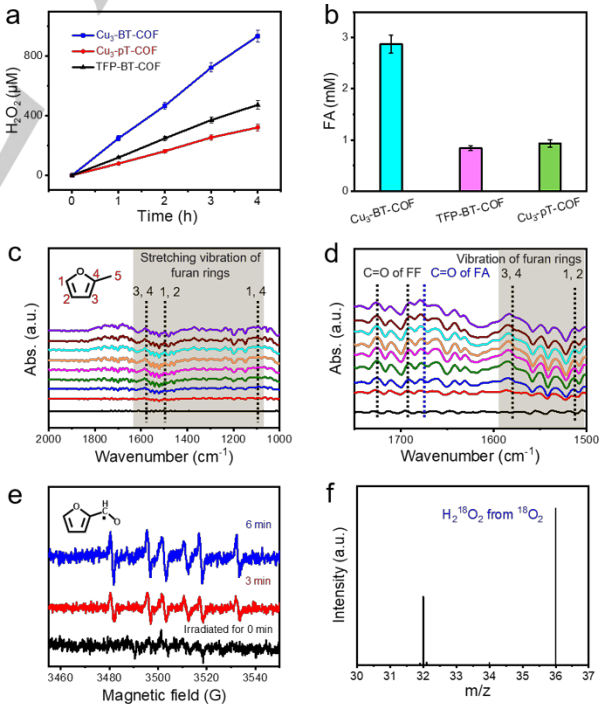

Figure 3. Photo-catalytic performances of Cu_3-BT-COF, Cu_3-pT-COF and TFP-BT-COF in H_2O_2 photosynthesis coupled with FFA photo-oxidation. (a) Photocatalytic activity of Cu_3-BT-COF, Cu_3-pT-COF and TFP-BT-COF for H_2O_2 photosynthesis. (b) Photocatalytic activity of Cu_3-BT-COF, Cu_3-pT-COF and TFP-BT-COF for FA photo-oxidation. (c), (d) DRIFTs spectra of FFA transformation during the photocatalytic reaction by Cu_3-BT-COF. (e) In the presence of Cu_3-BT-COF, EPR signals for *FF under different illumination time

This article is protected by copyright. All rights reserved.

15213773, ja, Downloaded from https://onlinelibrary.wiley.com/doi/10.1002/anie.202303606 by South China Normal University, Wiley Online Library on [13/06/2023]. See the Terms and Conditions (https://onlinelibrary.wiley.com/terms-and-conditions) on Wiley Online Library for rules of use; OA articles are governed by the applicable Creative Commons License

Accepted Manuscript

in the presence of DMPO as the spin-trapping reagent. (f) $^{18}O_2$ isotope experiment to explore the source of H_2O_2.

In order to study the involved mechanism of O_2 in the process of H_2O_2 photosynthesis coupled with FAA photo-oxidation, we have also studied the photocatalytic coupled system under different atmospheres. Specifically, the production rate for H_2O_2 photosynthesis under N_2 and air atmospheres are 110 μM g^{-1} and 11200 μM g^{-1}, respectively, which are much lower than that under O_2 atmosphere (187,000 μM g^{-1}) (Figure S42). In addition, the conversion of FFA under N_2 (~42 mM g^{-1}) and air (~164 mM g^{-1}) atmospheres are also much lower than that under O_2 atmosphere (~575 mM g^{-1}) (Figure S43). Furthermore, 5,5-dimethylpyrroline N-oxide (DMPO) is applied as a free radical spin trapping agent to determine *OH, $•O_2^-$ and active intermediate (*FF) in electron paramagnetic resonance (EPR) tests (Figure 3e).[11c] With the increase of illumination time (0 to 6 min), the typical characteristic peaks of DMPO-*FF and DMPO-*OH become stronger, which proves that *FF and *OH are produced during the process of photocatalysis. In addition, the typical characteristic signal for DMPO-$•O_2^-$ are markedly observed in the presence of Cu_3-BT-COF under light illumination (Figure S44), indicating the generation of $•O_2^-$ intermediate species. Specifically, all of the intermediates are absent under dark conditions in the presence of Cu_3-BT-COF, suggesting the vital role of light illumination during these processes. In order to study the mechanism of Cu_3-pT-COF and TFP-BT-COF, DMPO is also applied as a free radical spin trapping agent to carry out the EPR tests, and typical characteristic signals of *OH, $•O_2^-$ and *FF have been also observed under light illumination and absent under dark conditions (Figure S45-46).

To reveal the specific effects of electron-hole pairs and ROS (e.g., $•O_2^-$ and *OH) produced in this system, we have conducted a series of control experiments with the addition of different specific radical scavengers (Figure S47-48). When p-benzoquinone (BQ) is applied as a superoxide radical scavenger, the conversion efficiency is only ~34% with a low production rate of 196 mM g^{-1} for FFA to FA under standard conditions. Meanwhile, when isopropanol (IPA) is added as the hydroxyl scavenger and potassium iodide (KI) as the hole scavenger, the conversion efficiency of FFA reduces to 21% and 39%, and the product rate of FA is only 120 mM g^{-1} and 224 mM g^{-1}, respectively (Figure S47). When BQ, IPA and KI are utilized as free radical sacrificial agents, the production rate of H_2O_2 photosynthesis also decrease to 28,050 μM g^{-1}, 170,184 μM g^{-1} and 151,844 μM g^{-1}, respectively (Figure S48). The above results certify that ROS (e.g., $•O_2^-$ and *OH) and photogenerated holes are indeed involved in the H_2O_2 photosynthesis coupled with FFA photo-oxidation system.

In addition, we have performed the in-situ diffuse reflectance infrared Fourier transform spectroscopy (DRIFTs) measurements (Figure 3c). After the system is equilibrated, the peaks appeared at 1470~1560 cm^{-1} are attributed to the vibration of furan ring. In detail, the absorption peaks of 1146 cm^{-1}, 1507 cm^{-1} and 1588 cm^{-1} are ascribed to the vibration of C^1-O-C^4, C^1=C^2 and C^3=C^4 located on the furan ring, respectively, in which the order of C is marked and shown in Figure 3c. With the proceeding of the photocatalytic reaction, the absorption peaks (i.e. 1727 cm^{-1} and 1697 cm^{-1}) that ascribed to the furan ring in furfural (FF) emerges, implying the generation of the vital intermediate of FF (Figure 3d). The absorption peak located at 2860 cm^{-1} (attributed to methylene on FF) becomes stronger, further proving the production of furfural intermediates. (Figure S49).[11c,27] Gradually, the absorption peaks at 1167 cm^{-1} and 1678 cm^{-1} belonging to the vibration of FA becomes stronger, which suggests that FFA and FF are gradually oxidized to FA. [11c]

In order to further expand the types of photocatalytic coupled system reaction, we replace FFA oxidation with 2-thiophenemethanol (TM) oxidation. In the H_2O_2 photosynthesis coupled with TM photo-oxidation, after 4 h illumination, the conversion efficiency of TM can reach up to >97% by Cu_3-BT-COF, meanwhile H_2O_2 photosynthesis is relatively high (~162,400 μM g^{-1}) (Figure S50-54). In contrast, the performances of TFP-BT-COF and Cu_3-pT-COF are low than that of Cu_3-BT-COF (Figure S51).

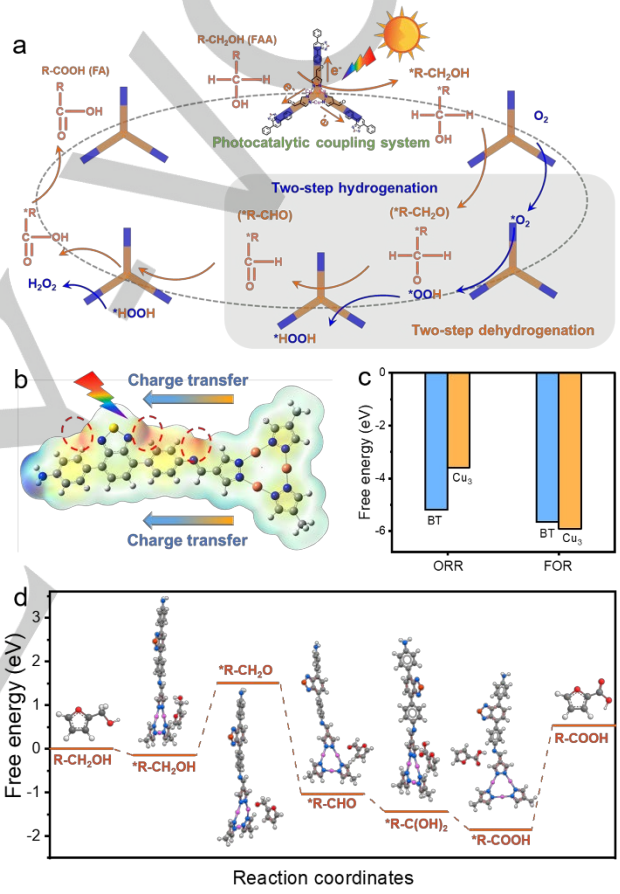

Figure 4. DFT calculations and the proposed reaction mechanism. (a) Schematic diagram of proposed reaction mechanism for H_2O_2 photosynthesis coupled with FAA photo-oxidation by Cu_3-BT-COF (the circled place represents the synergistic hydrogenation (H_2O_2 photosynthesis) and dehydrogenation (FFA photo-oxidation) processes) (R = furan ring). (b) Differential charge density diagram of Cu_3-BT-COF. (c) Adsorption energy of Cu_3 and BT units in Cu_3-BT-COF for FFA and O_2. (d) Free energy diagrams of FFA photo-oxidation steps on Cu_3-BT-COF.

Based on the above experiments and analysis, a possible mechanism is proposed to illustrate the H_2O_2 photosynthesis coupled with FAA photo-oxidation by Cu_3-BT-COF (Figure 4a).[10b,11c] To study the possible mechanism for the H_2O_2 photosynthesis coupled with FFA photo-oxidation, theoretical calculation has been conducted. Initially, the charge distribution of Cu_3-BT-COF structure is analyzed by differential charge

This article is protected by copyright. All rights reserved.

15213773, ja, Downloaded from https://onlinelibrary.wiley.com/doi/10.1002/anie.202303606 by South China Normal University, Wiley Online Library on [13/06/2023]. See the Terms and Conditions (https://onlinelibrary.wiley.com/terms-and-conditions) on Wiley Online Library for rules of use; OA articles are governed by the applicable Creative Commons License

Accepted Manuscript

density (Figure 4b). This result displays that the electrostatic potential value around BT is positive, indicating that this area is easier to obtain electrons and is more electrophilic than that of Cu_3. Thus, the result confirms our proposed mechanism that the oxidation and reduction reactions are more likely to occur on Cu_3 and BT, respectively (Figure 4a). Then, we also calculate the corresponding adsorption energies of FFA and O_2 on the possible adsorption sites of Cu_3 and BT units (Figure 4c). As shown in Figure 4c, the adsorption energies of FFA on Cu_3 and BT are -5.92 eV and -5.66 eV, respectively, which indicates that FFA is more easily adsorbed on Cu_3 than BT. Meanwhile, the adsorption energies of O_2 on Cu_3 and BT are -3.59 eV and -5.2 eV, respectively, which implies that O_2 is more easily adsorbed on BT than FFA. These results are consistent with the results of differential charge density.

Based on the above calculation results and analysis, we have calculated the free energy of ORR and FOR pathways for Cu_3-BT-COF (Figure 4d). Generally, the reaction of ORR to generate H_2O_2 includes three basic reactions (O_2 → $*O_2$ → *HOOH → HOOH, * represents the catalytic site), in which the last step (*HOOH → HOOH) is the rate determination step (RDS), and its energy barrier is -1.2 eV (Figure 4d). Specifically, the free energies corresponding to the formation of $*O_2$ and *HOOH are -0.29 eV and -1.38 eV, respectively. The generation of *HOOH from $*O_2$ corresponds to two hydrogenation steps, in which the hydrogen comes from the dehydrogenation of FFA. Based on the analysis of H_2O_2 production process, the RDS is the stepwise combination of O_2 with hydrogen removed from FFA photo-oxidation. This indicates the closely related RDS of H_2O_2 production and FFA photo-oxidation. In addition, the specific FFA-to-FA reaction pathway (*R-CH_2OH → *R-CH_2O → *R-CHO → *R-C$(OH)_2$ → *R-COOH → R-COOH, * represents the catalytic site) involves the oxidation of FFA along with (H^+/e^-) pairs. As shown in the free energy diagram (Figure 4d), the RDS is the first deprotonation process of α-hydrogen on FFA (*R-CH_2OH - H^+ + h^+ → *R-CH_2O) with an energy barrier of 1.5 eV. After that, the generation of *R-CHO (ΔG, 0.24 eV) happens, follows with the spontaneous conversion of *R-CHO into *R-C$(OH)_2$ (ΔG, -1.44 eV). Then, the adsorbed intermediate of *R-C$(OH)_2$ is further oxidized to obtain *R-COOH. Finally, *R-COOH is desorbed to generate FA (Figure 4d). Notably, H_2O_2 photosynthesis and FFA photo-oxidation are closely related. Based on the above calculation results, the FFA dehydrogenation step as the RDS step for FFA photo-oxidation is closely associated with the stepwise hydrogenation of O_2 for H_2O_2 photosynthesis.

Conclusion

In summary, a series of redox molecular junction COFs (i.e. Cu_3-BT-COF, Cu_3-pT-COF and TFP-BT-COF) with different functional groups have been synthesized and can be successfully applied for H_2O_2 photosynthesis coupled with FAA photo-oxidation. Among them, Cu_3-BT-COF as a kind of newly designed MCOF with nanosheet morphology (~1.25 nm) constructed by the covalent connection of Cu_3 and thiazole group (BT) exhibits the optimal photocatalytic coupled reaction properties. It is worth noting that the FA generation efficiency of Cu_3-BT-COF can be as high as 575 mM g^{-1} (conv. ~100% and sele. >99%) and meanwhile the H_2O_2 production rate can reach up to 187,000 μM g^{-1}, much higher than Cu_3-pT-COF, TFP-BT-COF and its monomers. As supported by the theoretical calculations, the FFA dehydrogenation step as the RDS step for FFA photo-oxidation is closely associated with the stepwise hydrogenation of O_2 for H_2O_2 photosynthesis, thus creating efficient coupled system for both H_2O_2 and FA generation. Furthermore, the covalent connection of Cu_3 and thiazole group can promote the charge-transfer, accelerate substrate activation and facilitate the FFA dehydrogenation, thus boosting the both reaction kinetics of H_2O_2 production and FFA photo-oxidation to increase the efficiency. In addition, the reaction presents high versatility and can be extended to other alcohol photo-oxidation systems like H_2O_2 photosynthesis coupled with 2-thiophenemethanol photo-oxidation. Considering the advantages of the coupled photocatalytic system, the excellent performance achieved in this work would pave a new way for the exploration of porous crystalline catalysts in this field.

Acknowledgements

This work was financially supported by the NSFC (Grants 22225109, 22071109, 22171139). Natural Science Foundation of Guangdong Province (No. 2023B1515020076). Postdoctoral Innovation Talent Support Program (BX20220116).

Conflict of Interest

The authors declare no conflict of interest.

Keywords: Redox molecular junction • Covalent organic frameworks • Biomass valorization • H_2O_2 Photosynthesis • Photosynthesis coupled systems

References

[1] a) M. Yan, Z. Wei, Z. Gong, B. Johannessen, G. Ye, G. He, J. Liu, S. Zhao, C. Cui, H. Fei, *Nat. Commun.* **2023**, *14*, 368; b) J. Chen, Q. Ma, X. Zheng, Y. Fang, J. Wang, S. Dong, *Nat. Commun.* **2022**, *13*, 2808; c) Y. Sun, L. Han, P. Strasser, *Chem. Soc. Rev*. **2020**, *49*, 6605-6631; d) R. J. Lewis, K. Ueura, X. Liu, Y. Fukuta, T. E. Davies, D. J. Morgan, L. Chen, J. Qi, J. Singleton, J. K. Edwards, S. J. Freakley, C. J. Kiely, Y. Yamamoto, G. J. Hutchings, *Science* **2022**, *376*, 615-620.

[2] a) Q. Zhang, X. Tan, N. M. Bedford, Z. Han, L. Thomsen, S. Smith, R. Amal, X. Lu, *Nat. Commun.* **2020**, *11*, 4181.

[3] a) J. M. Campos-Martin, G. Blanco-Brieva, J. L. G. Fierro, *Angew. Chem. Int. Ed.* **2006**, *45*, 6962-6984; b) A. Huang, R. S. Delima, Y. Kim, E. W. Lees, F. G. L. Parlane, D. J. Dvorak, M. B. Rooney, R. P. Jansonius, A. G. Fink, Z. Zhang, C. P. Berlinguette, *J. Am. Chem. Soc.* **2022**, *144*, 14548-14554; c) H. Hou, X. Zeng, X. Zhang, *Angew. Chem. Int. Ed.* **2020**, *59*, 17356-17376; d) P. Cao, X. Quan, X. Nie, K. Zhao, Y. Liu, S. Chen, H. Yu, J. G. Chen, *Nat. Commun*. **2023**, *14*, 172.

[4] a) K. Li, Q. Ge, Y. Liu, L. Wang, K. Gong, J. Liu, L. Xie, W. Wang, X. Ruan, L. Zhang, *Energy Environ. Sci.* **2023**, *16*, 1135-1145; b) Y. Shiraishi, T. Takii, T. Hagi, S. Mori, Y. Kofuji, Y. Kitagawa, S. Tanaka, S. Ichikawa, T. Hirai, *Nat. Mater.* **2019**, *18*, 985-993; c) Z. Zhang, T. Tsuchimochi, T. Ina, Y. Kumabe, S. Muto, K. Ohara, H. Yamada, S. L. Ten-no, T. Tachikawa, *Nat. Commun*. **2022**, *13*, 1499; d) C. Dong, Y. Yang, X. Hu, Y. Cho, G. Jang, Y. Ao, L. Wang, J. Shen, J. H. Park, K. Zhang, *Nat. Commun*. **2022**, *13*, 4982; e) C. Zhao, X. Wang, Y. Yin, W. Tian, G. Zeng, H. Li, S. Ye, L. Wu, J. Liu, *Angew. Chem. Int. Ed.* **2022**, *61*, e202218318.

This article is protected by copyright. All rights reserved.

15213773, ja, Downloaded from https://onlinelibrary.wiley.com/doi/10.1002/anie.202303606 by South China Normal University, Wiley Online Library on [13/06/2023]. See the Terms and Conditions (https://onlinelibrary.wiley.com/terms-and-conditions) on Wiley Online Library for rules of use; OA articles are governed by the applicable Creative Commons License

Accepted Manuscript

[5] M. Kou, Y. Wang, Y. Xu, L. Ye, Y. Huang, B. Jia, H. Li, J. Ren, Y. Deng, J. Chen, Y. Zhou, K. Lei, L. Wang, W. Liu, H. Huang, T. Ma, *Angew. Chem. Int. Ed.* **2022**, *61*, e202200413.

[6] H. Yang, C. Li, T. Liu, T. Fellowes, S. Y. Chong, L. Catalano, M. Bahri, W. Zhang, Y. Xu, L. Liu, W. Zhao, A. M. Gardner, R. Clowes, N. D. Browning, X. Li, A. J. Cowan, A. I. Cooper. *Nat. Nanotechnol.* **2023**, *18*, 307-315.

[7] a) J. H. Baek, T. M. Gill, H. Abroshan, S. Park, X. Shi, J. Nørskov, H. S. Jung, S. Siahrostami, X. Zheng, *Acs Energy Lett.* **2019**, *4*, 720-728; b) Z. Teng, Q. Zhang, H. Yang, K. Kato, W. Yang, Y.-R. Lu, S. Liu, C. Wang, A. Yamakata, C. Su, B. Liu, T. Ohno, *Nat. Catal.* **2021**, *4*, 374-384.

[8] a) X. Zeng, Y. Liu, Y. Kang, Q. Li, Y. Xia, Y. Zhu, H. Hou, M. H. Uddin, T. R. Gengenbach, D. Xia, C. Sun, D. T. McCarthy, A. Deletic, J. Yu, X. Zhang, *ACS Catal.* **2020**, *10*, 3697-3706; b) J. Ma, X. Peng, Z. Zhou, H. Yang, K. Wu, Z. Fang, D. Han, Y. Fang, S. Liu, Y. Shen, Y. Zhang, *Angew. Chem. Int. Ed.* **2022**, *61*, e202210856; c) Y.-X. Ye, J. Pan, F. Xie, L. Gong, S. Huang, Z. Ke, F. Zhu, J. Xu, G. Ouyang, *Proc. Natl. Acad. Sci.* **2021**, *118*, e2103964118.

[9] a) D. Esposito, M. Antonietti, *Chem. Soc. Rev.* **2015**, *44*, 5821-5835; b) A. J. Ragauskas, C. K. Williams, B. H. Davison, G. Britovsek, J. Cairney, C. A. Eckert, W. J. Frederick, J. P. Hallett, D. J. Leak, C. L. Liotta, J. R. Mielenz, R. Murphy, R. Templer, T. Tschaplinski, *Science* **2006**, *311*, 484-489; c) Z. Zong, S. Mazurkewich, C. S. Pereira, H. Fu, W. Cai, X. Shao, M. S. Skaf, J. Larsbrink, L. Lo Leggio, *Nat. Commun.* **2022**, *13*, 1449.

[10] a) P. Sudarsanam, E. Peeters, E. V. Makshina, V. I. Parvulescu, B. F. Sels, *Chem. Soc. Rev.* **2019**, *48*, 2366-2421; b) H. Wang, X. Liu, W. Yang, G. Mao, Z. Meng, Z. Wu, H.-L. Jiang, *J. Am. Chem. Soc.* **2022**, *144*, 22008-22017; c) X. Liu, B. Li, G. Han, X. Liu, Z. Cao, D.-e. Jiang, Y. Sun, *Nat. Commun.* **2021**, *12*, 1868.

[11] a) J. Luo, X. Wei, Y. Qiao, C. Wu, L. Li, L. Chen, J. Shi, *Adv. Mater.* **2023**, *35*, 2210110; b) Z. Tian, C. Han, Y. Zhao, W. Dai, X. Lian, Y. Wang, Y. Zheng, Y. Shi, X. Pan, Z. Huang, H. Li, W. Chen, *Nat. Commun.* **2021**, *12*, 2039; c) B. He, Z. Wang, P. Xiao, T. Chen, J. Yu, L. Zhang, *Adv. Mater.* **2022**, *34*, 2203225.

[12] D. Li, Y. Zhao, Y. Miao, C. Zhou, L.-P. Zhang, L.-Z. Wu, T. Zhang, *Adv. Mater.* **2022**, *34*, 2207793.

[13] H. G. Cha, K.-S. Choi, *Nat. Chem.* **2015**, *7*, 328-333.

[14] J. Low, B. Dai, T. Tong, C. Jiang, J. Yu, *Adv. Mater.* **2019**, *31*, 1802981.

[15] a) X. Tian, Y. Guo, W. An, Y.-L. Ren, Y. Qin, C. Niu, X. Zheng, *Nat. Commun.* **2022**, *13*, 6186; b) B. Zhou, J. Song, Z. Zhang, Z. Jiang, P. Zhang, B. Han, *Green Chem.* **2017**, *19*, 1075-1081.

[16] a) Y. Yuan, K.-T. Bang, R. Wang, Y. Kim, *Adv. Mater.* **2023**, *35*, 2210952; b) M. Leng, L. Fang, *Chem* **2022**, *8*, 2904-2906; c) S. Kandambeth, K. Dey, R. Banerjee, *J. Am. Chem. Soc.* **2019**, *141*, 1807-1822; d) S. Zhao, C. Jiang, J. Fan, S. Hong, P. Mei, R. Yao, Y. Liu, S. Zhang, H. Li, H. Zhang, C. Sun, Z. Guo, P. Shao, Y. Zhu, J. Zhang, L. Guo, Y. Ma, J. Zhang, X. Feng, F. Wang, H. Wu, B. Wang, *Nat. Mater.* **2021**, *20*, 1551-1558; e) A. P. Côté, A. I. Benin, N. W. Ockwig, M. O'Keeffe, A. J. Matzger, O. M. Yaghi, *Science* **2005**, *310*, 1166-1170.

[17] a) J. Dong, X. Han, Y. Liu, H. Li, Y. Cui, *Angew. Chem. Int. Ed.* **2020**, *59*, 13722-13733; b) J. Luo, X. Luo, M. Xie, H.-Z. Li, H. Duan, H.-G. Zhou, R.-J. Wei, G.-H. Ning, D. Li, *Nat. Commun.* **2022**, *13*, 7771; c) J.-N. Chang, Q. Li, Y. Yan, J.-W. Shi, J. Zhou, M. Lu, M. Zhang, H.-M. Ding, Y. Chen, S.-L. Li, Y.-Q. Lan, *Angew. Chem. Int. Ed.* **2022**, *61*, e202209289; d) R.-J. Wei, P.-Y. You, H. Duan, M. Xie, R.-Q. Xia, X. Chen, X. Zhao, G.-H. Ning, A. I. Cooper, D. Li, *J. Am. Chem. Soc.* **2022**, *144*, 17487-17495.

[18] J. Zhou, J. Li, L. Kan, L. Zhang, Q. Huang, Y. Yan, Y. Chen, J. Liu, S.-L. Li, Y.-Q. Lan, *Nat. Commun.* **2022**, *13*, 4681.

[19] J. Francis Kurisingal, H. Kim, J. Hyeak Choe, C. Seop Hong, *Coord. Chem. Rev.* **2022**, *473*, 214835.

[20] a) D. M. Flores, M. L. Neville, V. A. Schmidt, *Nat. Commun.* **2022**, *13*, 2764; b) G. K. Jayasekara, C. Antolini, M. A. Smith, D. J. Jacoby, J. Escolastico, N. Girard, B. T. Young, D. Hayes, *J. Am. Chem. Soc.* **2021**, *143*, 19356-19364.

[21] X. Li, J. Wang, F. Xue, Y. Wu, H. Xu, T. Yi, Q. Li, *Angew. Chem. Int. Ed.* **2021**, *60*, 2534-2540.

[22] J. Liu, Y. Liu, N. Liu, Y. Han, X. Zhang, H. Huang, Y. Lifshitz, S.-T. Lee, J. Zhong, Z. Kang, *Science* **2015**, *347*, 970-974.

[23] a) Y. Kofuji, Y. Isobe, Y. Shiraishi, H. Sakamoto, S. Tanaka, S. Ichikawa, T. Hirai, *J. Am. Chem. Soc.* **2016**, *138*, 10019-10025; b) J. García-Serna, T. Moreno, P. Biasi, M. J. Cocero, J.-P. Mikkola, T. O. Salmi, *Green Chem.* **2014**, *16*, 2320-2343.

[24] Y.-R. Wang, H.-M. Ding, X.-Y. Ma, M. Liu, Y.-L. Yang, Y. Chen, S.-L. Li, Y.-Q. Lan, *Angew. Chem. Int. Ed.* **2022**, *61*, e202114648.

[25] Z. Wei, M. Liu, Z. Zhang, W. Yao, H. Tan, Y. Zhu, *Energy Environ. Sci.* **2018**, *11*, 2581-2589.

[26] a) Hu, W.-Y.; Li, Q.-Y.; Zhai, G.-Y.; Lin, Y.-X.; Li, D.; He, X.-X.; Lin, X.; Xu, D.; Sun, L.-H.; Zhang, S.-N.; Chen, J.-S.; Li, X.-H., *Small* **2022**, *18*, 2200885; b) Zheng, Y.; Zhou, H.; Zhou, B.; Mao, J.; Zhao, Y., *Catal. Sci. Technol.* **2022**, *12*, 969-975; c) Chen, X.; Kondo, Y.; Li, S.; Kuwahara, Y.; Mori, K.; Zhang, D.; Louis, C.; Yamashita, H., *J. Mater. Chem. A*, **2021**, *9*, 26371-26380.

[27] S. Li, Y. Fan, C. Wu, C. Zhuang, Y. Wang, X. Li, J. Zhao, Z. Zheng, *ACS Appl. Mater. Interfaces* **2021**, *13*, 8507-8517.

This article is protected by copyright. All rights reserved.

15213773, ja, Downloaded from https://onlinelibrary.wiley.com/doi/10.1002/anie.202303606 by South China Normal University, Wiley Online Library on [13/06/2023]. See the Terms and Conditions (https://onlinelibrary.wiley.com/terms-and-conditions) on Wiley Online Library for rules of use; OA articles are governed by the applicable Creative Commons License

Accepted Manuscript

10.1002/anie.202303606

Entry for the Table of Contents

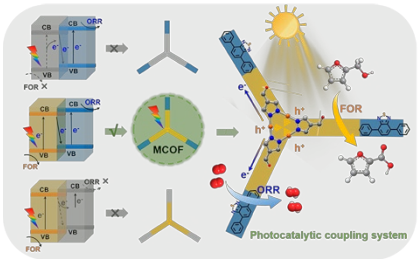

A series of covalent organic frameworks with well-tuned redox molecular junctions have been prepared and can be successfully applied for H_2O_2 photosynthesis coupled with furfuryl alcohol photo-oxidation.

This article is protected by copyright. All rights reserved.

15213773, ja, Downloaded from https://onlinelibrary.wiley.com/doi/10.1002/anie.202303606 by South China Normal University, Wiley Online Library on [13/06/2023]. See the Terms and Conditions (https://onlinelibrary.wiley.com/terms-and-conditions) on Wiley Online Library for rules of use; OA articles are governed by the applicable Creative Commons License

Accepted Manuscript